Research Articles

Association of *Fusobacterium nucleatum* with Specific T Cell Subsets in the Colorectal Carcinoma Microenvironment

Authors:
Jennifer Borowsky,[1,2,3,4] Koichiro Haruki,[1,5] Mai Chan Lau,[1,5] Andressa Dias Costa,[6] Juha P. Väyrynen,[1,5,6,7] Tomotaka Ugai,[1,8] Kota Arima,[1,5] Annacarolina da Silva,[5] Kristen D. Felt,[9] Melissa Zhao,[5] Carino Gurjao,[6] Tyler S. Twombly,[1,5] Kenji Fujiyoshi,[1,5] Sara A. Väyrynen,[5,6] Tsuyoshi Hamada,[1,5] Kosuke Mima,[5] Susan Bullman,[10] Tabitha A. Harrison,[11] Amanda I. Phipps,[11,12] Ulrike Peters,[11,12] Kimmie Ng,[6] Jeffrey A. Meyerhardt,[6] Mingyang Song,[13,14,15] Edward L. Giovannucci,[8,13] Kana Wu,[8,13,16] Xuehong Zhang,[16] Gordon J. Freeman,[6] Curtis Huttenhower,[17,18] Wendy S. Garrett,[6,18,19] Andrew T. Chan,[14,15,16,19] Barbara A. Leggett,[3,4,20] Vicki L. J. Whitehall,[3,4,21] Neal Walker,[4,22] Ian Brown,[4,22] Mark Bettington,[3,4,22] Reiko Nishihara,[1,5,8,13,17] Charles S. Fuchs,[23,24,25] Jochen K. Lennerz,[2] Marios Giannakis,[6,18,26] Jonathan A. Nowak,[1] and Shuji Ogino[1,5,8,18,27]

J.B., K.H., M.C.L., and A.D.C. contributed equally as co-first authors.
J.K.L., M.G., J.A.N., and S.O. contributed equally as co-last authors.

Author Affiliations:
[1] Department of Oncologic Pathology, Dana-Farber Cancer Institute and Harvard Medical School, Boston, MA; [2] Department of Pathology, Center for Integrated Diagnostics, Massachusetts General Hospital and Harvard Medical School, Boston, MA; [3] Conjoint Gastroenterology Laboratory, QIMR Berghofer Medical Research Institute, Brisbane, Queensland, Australia; [4] School of Medicine, The University of Queensland, Brisbane, Queensland, Australia; [5] Program in MPE Molecular Pathological Epidemiology, Department of Pathology, Brigham and Women's Hospital and Harvard Medical School, Boston, MA; [6] Department of Medical Oncology, Dana-Farber Cancer Institute and Harvard Medical School, Boston, MA; [7] Cancer and Translational Medicine Research Unit, Medical Research Center Oulu, Oulu University Hospital, and University of Oulu, Oulu, Finland; [8] Department of Epidemiology, Harvard T.H. Chan School of Public Health, Boston, MA; [9] Center for Immuno-Oncology, Dana-Farber Cancer Institute, Boston, MA; [10] Human Biology Division, Fred Hutchinson Cancer Research Center, Seattle, WA; [11] Public Health Sciences Division, Fred Hutchinson Cancer Research Center, Seattle, WA; [12] Department of Epidemiology, University of Washington, Seattle, WA; [13] Department of Nutrition, Harvard T.H. Chan School of Public Health, Boston, MA; [14] Clinical and Translational Epidemiology Unit, Massachusetts General Hospital and Harvard Medical School, Boston, MA; [15] Division of Gastroenterology, Massachusetts General Hospital, Boston, MA; [16] Channing Division of Network Medicine, Department of Medicine, Brigham and Women's Hospital and Harvard Medical School, Boston, MA; [17] Department of Biostatistics, Harvard T.H. Chan School of Public Health, Boston, MA; [18] Broad Institute of MIT and Harvard, Cambridge, MA; [19] Department of Immunology and Infectious Diseases, Harvard T.H. Chan School of Public Health, Boston, MA; [20] The Royal Brisbane and Women's

Hospital, Brisbane, Queensland, Australia; [21] Conjoint Internal Medicine Laboratory, Pathology Queensland, Queensland Health, Brisbane, Queensland, Australia; [22] Envoi Specialist Pathologists, Brisbane, Queensland, Australia; [23] Yale Cancer Center, New Haven, CT; [24] Department of Medicine, Yale School of Medicine, New Haven, CT; [25] Smilow Cancer Hospital, New Haven, CT; [26] Department of Medicine, Brigham and Women's Hospital and Harvard Medical School, Boston, MA; [27] Cancer Immunology and Cancer Epidemiology Programs, Dana-Farber Harvard Cancer Center, Boston, MA.

Running Title: *Fusobacterium* and T Cell Subsets in CRC

Keywords: colorectal neoplasms; immunology; microbiome; molecular pathological epidemiology; tumor microenvironment.

Co-corresponding authors:

Jonathan A. Nowak, MD, PhD
Program in MPE Molecular Pathological Epidemiology,
Department of Pathology,
Brigham and Women's Hospital
75 Francis Street, Boston, MA 02115
Tel: 617-732-7641
Email: janowak@bwh.harvard.edu

Shuji Ogino, MD, PhD, MS
Program in MPE Molecular Pathological Epidemiology,
Department of Pathology,
Brigham and Women's Hospital
221 Longwood Ave., Room EBRC404, Boston, MA, 02215
Tel: 617-525-8953; Fax: 617-264-5149
E-mail: sogino@bwh.harvard.edu

Disclosure of Potential Conflicts of Interest: J.A.M. has received institutional research funding from Boston Biomedical, has served as an advisor/consultant to Ignyta and COTA Healthcare, and served on a grant review panel for the National Comprehensive Cancer Network funded by Taiho Pharmaceutical. A.T.C. previously served as a consultant for Bayer Healthcare and Pfizer Inc.. R.N. is currently employed by Pfizer Inc.; she contributed to this study before she became an employee of Pfizer Inc.. M.G. receives research funding from Bristol-Myers Squibb and Merck. C.S.F. previously served as a consultant for Agios, Bain Capital, Bayer, Celgene, Dicerna, Five Prime Therapeutics, Gilead Sciences, Eli Lilly, Entrinsic Health, Genentech, KEW, Merck, Merrimack Pharmaceuticals, Pfizer Inc, Sanofi, Taiho, and Unum Therapeutics; C.S.F. also serves as a Director for CytomX Therapeutics and owns unexercised stock options for CytomX and Entrinsic Health. G.J.F. reports grants from National Cancer Institute during the conduct of the study; personal fees from Roche, personal fees from Bristol-Myers Squibb, personal fees from Xios, personal fees from Orogimed, personal fees from Triursus, personal fees from iTeos, personal fees from NextPoint, personal

fees from IgM, personal fees from Jubilant, personal fees from GV20, and personal fees from Trillium outside the submitted work. In addition, G.J.F. has a patent for CD274 (PD-L1) / PDCD1 (PD-1) pathway issued, licensed, and with royalties paid from Roche, a patent for CD274 (PD-L1)/PDCD1 (PD-1) pathway issued, licensed, and with royalties paid from Merck MSD, a patent for CD274 (PD-L1)/PDCD1 (PD-1) pathway issued, licensed, and with royalties paid from Bristol-Myers-Squibb, a patent for CD274 (PD-L1)/PDCD1 (PD-1) pathway issued, licensed, and with royalties paid from Merck KGA, a patent for CD274 (PD-L1)/PDCD1 (PD-1) pathway issued, licensed, and with royalties paid from Astra-Zeneca, a patent for CD274 (PD-L1)/PDCD1 (PD-1) pathway issued, licensed, and with royalties paid from Dako, a patent for CD274 (PD-L1)/PDCD1 (PD-1) pathway issued, licensed, and with royalties paid from Mayo Clinic, and a patent for CD274 (PD-L1)/PDCD1 (PD-1) pathway issued, licensed, and with royalties paid from Novartis. G.J.F. has equity in Nextpoint, Triursus, Xios, iTeos, IgM, GV20, and Geode. This study was not funded by any of these commercial entities. The other authors declare that they have no conflicts of interest.

Word count (text): 3,994 words
Figures and tables: 1 figure, 5 tables, 2 supplementary tables, and 1 supplementary figure.

Abbreviations: AJCC, American Joint Committee on Cancer; CI, confidence interval; CIMP, CpG island methylator phenotype; FFPE, formalin-fixed paraffin-embedded; HPFS, Health Professionals Follow-up Study; IPW, inverse probability weighting; LINE-1, long-interspersed nucleotide element-1; MSI, microsatellite instability; NHS, Nurses' Health Study; OR, odds ratio; PCR, polymerase chain reaction; SD, standard deviation; TAM, tumor-associated macrophage.

Use of Standardized Official Symbols: We use HUGO (Human Genome Organisation)-approved official symbols (or root symbols) for genes and gene products, including BRAF, CACNA1G, CD3, CD4, CD8, CD68, CD86, CD274, CDH1, CDKN2A, CRABP1, CTNNB1, FOXP3, IGF2, IRF5, KRAS, KRT, MAF, MLH1, MRC1, NEUROG1, PDCD1, PIK3CA, PTPRC, RUNX3, SOCS1, TIGIT, and WNT; all of which are described at www.genenames.org. Gene symbols are italicized whereas symbols for gene products are not italicized.

Author Contributions:
J.B., K.H., M.C.L., and A.D.C. contributed equally, and J.K.L., M.G., J.A.N., and S.O. contributed equally.
J.B., K.H., J.A.N., and S.O. had full access to all of the data in the study and take responsibility for the integrity of the data and the accuracy of the data analysis.
Study concept and design: J.K.L., M.G., J.A.N., and S.O.
Acquisition, analysis, or interpretation of data: J.B., K.H., A.D.C., J.P.V., K.A., C.G., K.M., J.A.M., M.S., A.T.C., R.N., C.S.F., J.A.N., and S.O.
Drafting of the manuscript: J.B., K.H., M.C.L., J.P.V., and S.O.
Critical revision of the manuscript for important intellectual content: All authors.
Statistical analysis: J.B., K.H., M.C.L., J.P.V., T.U., R.N., C.S.F., and S.O.

Obtained funding: K.N., C.H., W.S.G., M.G., A.T.C., C.S.F., and S.O.
Administrative, technical, or material support: J.B., K.H., J.P.V., R.N., A.T.C., C.H., W.S.G., C.S.F., and S.O.
Study supervision: J.K.L., M.G., J.A.N., and S.O.

Translational Relevance

Our multiplex immunofluorescence assay combined with digital image analyses and machine learning enabled us to robustly quantify T-cell subsets in 933 colorectal cancer cases within a large database of 4,465 incident colorectal cancers in two prospective U.S.-wide cohort studies. We found an inverse association of *Fusobacterium nucleatum* DNA amount with tumor stromal density of $CD3^{+}CD4^{+}CD45RO^{+}$ helper memory T cells. Fewer memory T cells may contribute to a lack of immune attack on developing tumors. Our unique human population-based evidence for microbial-immune interactions supports possible interventions targeting the microbiota and/or immunity for cancer prevention and therapy.

Abstract

Purpose: While evidence indicates that *Fusobacterium nucleatum* may promote colorectal carcinogenesis through its suppressive effect on T-cell-mediated antitumor immunity, the specific T-cell subsets involved remain uncertain.

Experimental Design: We measured *F. nucleatum* DNA within tumor tissue by quantitative PCR on 933 cases (including 128 *F. nucleatum*-positive cases) among 4,465 incident colorectal carcinoma cases in two prospective cohorts. Multiplex immunofluorescence combined with digital image analysis and machine learning algorithms for CD3, CD4, CD8, CD45RO (PTPRC isoform), and FOXP3 measured various T-cell subsets. We leveraged data on *Bifidobacterium*, microsatellite instability (MSI), tumor whole exome sequencing, and M1/M2-type tumor-associated macrophages [by CD68, CD86, IRF5, MAF, and MRC1 (CD206) multimarker assay]. Using the 4,465 cancer cases and inverse probability weighting method to control for selection bias due to tissue availability, multivariable-adjusted logistic regression analysis assessed the association between *F. nucleatum* and T-cell subsets.

Results: The amount of *F. nucleatum* was inversely associated with tumor stromal $CD3^+$ lymphocytes (multivariable odds ratio, 0.47, 95% confidence interval, 0.28-0.79, for *F. nucleatum*-high vs. negative category; P_{trend}=0.0004) and specifically stromal $CD3^+CD4^+CD45RO^+$ cells (corresponding multivariable odds ratio, 0.52, 95% confidence interval, 0.32-0.85; P_{trend}=0.003). These relationships did not substantially

differ by MSI status, neoantigen loads, or exome-wide tumor mutational burden. *F. nucleatum* was not significantly associated with tumor intraepithelial T cells or with M1 or M2 tumor-associated macrophages.

Conclusions: The amount of tissue *F. nucleatum* is associated with lower densities of stromal memory helper T cells. Our findings provide evidence for the interactive pathogenic roles of microbiota and specific immune cells.

Introduction

Accumulating evidence indicates the complex role of the microbiota and host immunity in carcinogenesis (1-4). As T cell-mediated adaptive immune response influences tumor development (5,6), immunotherapies targeting immune checkpoints that regulate T cell activity have emerged as promising treatment strategies for various types of malignancy, including colorectal cancer (7-9). In colorectal cancer, high densities of tumor-infiltrating immune cells, including $CD3^+$ cells, $CD8^+$ cells, and $CD45RO^+$ cells have been associated with better survival (10-12). Recent advances in multiplex immunofluorescence technologies enable detailed evaluation of cellular phenotype as well as information on spatial distribution of each cell in relation to tumor epithelium and stroma, thereby providing deeper insights into the tumor immune microenvironment (13).

Fusobacterium nucleatum (*F. nucleatum*), Gram-negative anaerobic bacterium, is near ubiquitous in the oral cavity yet rarely found in other anatomic sites under healthy conditions (14,15). In disease states it has been identified in various extra-oral sites with studies demonstrating an enrichment of *F. nucleatum* in colorectal carcinoma tissue compared to adjacent normal tissue (16-18). Experimental studies have shown that *F. nucleatum* activates the WNT/CTNNB1 (beta-catenin) signaling pathway in colorectal cancer cells, promotes tumor growth (19,20), and inhibits T cell-mediated immune responses against colorectal cancer (20,21). Consistent with these findings, a higher amount of *F. nucleatum* DNA in colorectal cancer tissue has been associated with advanced disease stage, worse survival, and lower T cell density in tumor (18,22).

However, the relationship between *F. nucleatum* and specific T cell subsets in the colorectal tumor microenvironment have not been well-defined.

Using a multiplex assay that allows detailed characterisation of T cells and their spatial localisation within tumor intraepithelial and stromal regions, this analysis represents among the first human studies to test the hypothesis that *F. nucleatum* DNA amount in tumor tissue might be inversely associated with specific T cell subset densities.

Methods

Study Population

We utilized data from two prospective cohort studies in the U.S., the Nurses' Health Study (NHS, 121,701 women aged 30-55 years followed since 1976) and the Health Professionals Follow-up Study (HPFS, 51,529 men aged 40-75 years followed since 1986) (22-24). Study participants have been sent questionnaires biennially to update information on lifestyle factors and newly-diagnosed diseases including colorectal cancer. The follow-up rate has been more than 90% for each follow-up questionnaire cycle in both cohort studies. In both studies, the National Death Index was used to ascertain deaths of study participants and identify unreported lethal colorectal cancer cases. Study physicians, who were blinded to exposure data, reviewed medical records of identified colorectal cancer cases to confirm the disease

diagnosis and to collect data on tumor size, tumor anatomical location, and disease stage based on the American Joint Committee on Cancer TNM classification. We included both colon and rectal carcinomas based on the colorectal continuum model (25). In the cohort studies, 4,465 incident colorectal carcinoma cases had been documented up to 2012. We attempted to collect formalin-fixed paraffin-embedded (FFPE) tumor tissue blocks from hospitals throughout the U.S. (where colorectal cancer patients had undergone surgical resection), resulting in 933 cases with sufficient tissue and T-cell data. A single pathologist (S.O.), blinded to other data, reviewed hematoxylin and eosin-stained tissue sections and recorded pathological features. Tumor differentiation was categorized into well/moderate vs. poor (> 50% vs. ≤ 50% gland formation, respectively).

The study was conducted in accordance with the U.S. Common Rule. All participants gave written informed consent for the study. This study was approved by the institutional review boards of Brigham and Women's Hospital and Harvard T.H. Chan School of Public Health (Boston, MA), and those of participating registries as required.

Multiplex Immunofluorescence Analyses for T Cells and Macrophages in Tumor

We constructed tissue microarrays of colorectal cancer cases with sufficient tissue materials, including up to four tumor cores from each case in a tissue microarray block (26). As previously described (27,28), 4 μm sections from tissue microarray blocks were sequentially stained using the following antibodies/fluorescent dyes for T

cell, in order: anti-CD3 antibody (clone F7.2.38; Dako; Agilent Technologies, Carpenteria, CA)/Opal-520, anti-FOXP3 (clone 206D, Biolegend, San Diego, CA, USA)/Opal-540, anti-CD45RO (one of PTPRC isoforms) (clone UCHL1, Dako)/Opal-650, anti-CD8 (clone C8/144B, Dako)/Opal-570, anti-CD4 (clone 4B12, Dako)/Opal-690, anti-KRT (keratin, pan-cytokeratins) (clone AE1/AE3, Dako, and clone C11, Cell signaling, Danvers, MA)/Opal-620 (**Supplementary Figure S1**) [with standardized protein nomenclature recommended by a panel of experts (29)].

Digital images of all tissue microarray cores were acquired at 200x magnification using the Vectra multispectral imaging platform (Vectra 3.0, Akoya Biosciences Hopkinton, MA). Images of each core underwent tissue segmentation to characterize regions of tumor epithelium and peritumoral stroma based on cytokeratin expression using supervised machine learning algorithms within Inform 2.4.1 (Akoya Biosciences). Following tissue segmentation, cell enumeration and segmentation was performed using the DAPI signal to aid in identification of nuclei (**Supplementary Figure S1**). We evaluated Comparison of T-cell subset densities between the initial and re-processed data demonstrated a high degree of concordance (Pearson's *r* 0.48-0.99, Spearman's *r* 0.77-0.99) between the density measurements. Each cell was further segmented into nuclear, cytoplasmic and membranous compartments. A separate supervised machine learning algorithm was used to identify T cells based upon a combination of cytomorphology and subcellular T cell marker expression patterns. We evaluated self-reproducibility and the reliability of tissue segmentation and T cell identification using supervised machine learning and confirmed a high degree of concordance (J.B.). We also evaluated pathologist-to-pathologist (J.B. and A.D.C.) concordance through their

independent analyses starting from raw multispectral image data and confirmed moderate to high concordance. This single cell data was then used to calculate T cell subpopulation densities within separate regions. Aggregate tumor-level densities were then determined by calculating the average density for each subset across all regions from each tumor. T cell densities were initially classified into quartile categories (C1-C4). If more than 25% of all cases had zero density of a specific cell type, these zero-value cases were grouped together (C1 category), and the remaining (non-zero-value) cases were divided into tertile categories according to density (C2 to C4).

In exploratory analyses, we evaluated tumor-associated macrophage (TAM) densities and polarization using a separate multiplex immunofluorescence panel that included a pan-macrophage marker (CD68), two markers generally expressed in M1 TAMs (CD86, IRF5), two markers generally expressed in M2 TAMs [MAF, MRC1 (CD206)], a tumor cell marker [KRT, (keratin)], and DAPI, as previously described (30). We calculated an M1:M2 polarization index using the formula "(CD86 × IRF5) / (MRC1 × MAF)" based on the expression level of each protein. The TAMs within the highest 30% of the index were regarded as M1-like TAMs, while the macrophages within the lowest 30% were regarded as M2-like TAMs for these analyses, according to our previous study (30). We calculated each cell density (cell count per mm^2) in tumor intraepithelial and stromal regions separately, and macrophage densities were classified into quartile categories (C1-C4).

DNA Analyses for *Fusobacterium nucleatum* and *Bifidobacterium* genus in Tumor

Genomic DNA was extracted from archival FFPE tissue sections of colorectal carcinoma using the QIAamp DNA FFPE Tissue Kit (Qiagen, Hilden, Germany). As previously described (18,31), we performed quantitative polymerase chain reaction (PCR) assays to measure the amounts of *F. nucleatum* and *Bifidobacterium* genus DNA in tumor tissue, using *SLCO2A1* (for *F. nucleatum*) or a universal 16S primer set (for *Bifidobacterium* genus) as reference genes. Cases with any detectable *F. nucleatum* DNA (or *Bifidobacterium* genus) were categorized as low vs. high based on the median level of *F. nucleatum* (or *Bifidobacterium* genus), while cases without detectable *F. nucleatum* (or *Bifidobacterium* genus) were categorized as negative.

Evaluation of Tumor Molecular Characteristics

Tumor MSI status was analyzed using PCR of 10 microsatellite markers (D2S123, D5S346, D17S250, BAT25, BAT26, BAT40,D18S55, D18S56, D18S67, and D18S487), and MSI-high was defined as presence of instability in ≥ 30% of the markers, as previously described (24,28,32). Using bisulfite-treated DNA, methylation status of eight CpG island methylator phenotype (CIMP)-specific promoters (*CACNA1G*, *CDKN2A*, *CRABP1*, *IGF2*, *MLH1*, *NEUROG1*, *RUNX3*, and *SOCS1*) and long interspersed nucleotide element-1 (LINE-1) was determined as previously described (24,28,32). CIMP-high was defined as ≥ 6 methylated promoters of eight promoters, and CIMP-low/negative as 0-5 methylated promoters as previously described (24,28,32). PCR and pyrosequencing were performed for *KRAS* (codons 12, 13, 61, and 146), *BRAF* (codon 600), and *PIK3CA* (exons 9 and 20), as previously described

(23,24,28,33). Whole exome sequencing was performed using DNA from tumor and matched normal tissue pairs, as previously described (34). Exome-wide tumor mutational burden was defined as the number of nonsynonymous somatic mutations identified per megabase in the sequenced exome. Using a neoantigen prediction pipeline for somatic mutations, the neoantigen loads (i.e., the number of proteins that likely give rise to immunogenic peptides in the tumor microenvironment) was estimated by counting peptides that bind to personal human leukocyte antigen molecules with high affinity (< 500 nM). Using NetMHCpan (version 2.4) (35), we predicted the binding affinities of all possible 9- and 10-mer mutant peptides to the corresponding human leukocyte antigen alleles inferred by the POLYSOLVER algorithm), as previously described (28,34). Based on all colorectal cancers with available whole exome sequencing data, neoantigen loads and exome-wide tumor mutational burden were divided into quartiles (Q1 to Q4).

Statistical Analysis

All statistical analyses were conducted using SAS software (version 9.4, SAS Institute, Cary, NC), and all *P* values were two-sided. We used the two-sided α level of 0.005 as recommended (36). The current study started specific primary hypothesis testing that was an assessment of a statistical trend of the association of the amount of *F. nucleatum* DNA (negative, low, and high; as an ordinal predictor variable) with each T cell subset density (an ordinal outcome variable). All other analyses represented secondary analyses. In secondary analyses to assess the association between *F.*

nucleatum DNA amount and each of categorical clinicopathological variables, the chi-square test was performed. To compare continuous variables, an analysis of variance assuming equal variances or Spearman correlation test was performed.

For our primary hypothesis testing, we conducted initial analyses to select T cell subset variables using Spearman's correlation tests that assessed the correlations of *F. nucleatum* DNA amount with densities of T cell subsets. To control for selection bias due to tissue data availability, we used inverse probability weighting (IPW) method (24,37), which used 4,465 incident colorectal cancer cases including the 933 cases with tissue data. First, we constructed a multivariable logistic regression model that had covariates as predictors and tissue data availability as an outcome variable. Based on the fitted regression model using all of the 4,465 cases, we calculated the probability of tissue availability in each case with a set of covariates. Then, each of 933 tissue data-available cases was weighted by the inverse of the probability. Weights greater than the 95th percentile were truncated and set to the value of the 95th percentile to reduce outlier effects (37). We confirmed that results without weight truncation did not differ substantially from those with weight truncation (data not shown). The logistic regression analyses without IPW yielded similar results (**Supplementary Table S1**) to the IPW-adjusted model.

To control for confounding, multivariable IPW-adjusted logistic regression analyses initially included sex (female vs. male), age at diagnosis (continuous), year of diagnosis (continuous), family history of colorectal cancer in any first-degree relative (present vs. absent), tumor location (proximal colon vs. distal colon vs. rectum), MSI status (MSI-high vs. non-MSI-high), CIMP status (high vs. low/negative), LINE-1

methylation level (continuous), *KRAS* status (mutant vs. wild-type), *BRAF* status (mutant vs. wild-type), and *PIK3CA* status (mutant vs. wild-type). A backward elimination was conducted with a threshold *P* of 0.20 to select variables for the final models. Cases with missing data [family history of colorectal cancer in a first-degree relative (0.9%), tumor location (0.4%), MSI (2.9%), CIMP (7.0%), *KRAS* (2.9%), *BRAF* (2.0%), and *PIK3CA* mutation (8.5%)] were included in the majority category of a given categorical covariate to limit the degrees of freedom of the models. For the cases with missing data on LINE-1 methylation (2.7%), we assigned a separate indicator variable. We confirmed that excluding the cases with missing information in any of the covariates did not substantially alter results (data not shown). The proportional odds assumption was assessed using the ordinal logistic regression model using the ordinal categories of T cell subset density (negative and tertile or quartile; as an ordinal outcome variable). We observed evidence of violation of this assumption in $CD3^+CD4^+$ cells, while those assumption in the other subsets were generally satisfied ($P > 0.07$). Therefore, for $CD3^+CD4^+$ cells, we used binary variable dichotomized at the median value as the outcome variable in logistic regression analysis.

In secondary analyses, we assessed the statistical interaction between *F. nucleatum* status in colorectal cancer tissue (negative, low, and high) and MSI status (high vs. non-high), neoantigen loads [high (Q3-4) vs. low (Q1-2)], or exome-wide tumor mutational burden [high (Q3-4) vs. low (Q1-2)] in relation to T cell subset densities. We used the Wald test for the cross-product in multivariable-adjusted logistic regression models. We estimated the odds ratio for a unit increase in the three ordinal categories of the amount of *F. nucleatum* in strata of MSI status, neoantigen loads, or exome-wide

tumor mutational burden using re-parameterization of the interaction term in a single regression model (32). For interaction analyses, the proportional odds assumption in an ordinal logistic regression model was violated in subpopulations defined by MSI status, neoantigen loads, and exome-wide tumor mutational burden, therefore we used binary outcome variables for all of the T cell measurements.

As exploratory analyses, we performed Spearman's correlation tests that assessed the correlation between *F. nucleatum* and TAMs densities. We further assessed the association of *Bifidobacterium* genus with T cell subset densities.

Results

During the longitudinal follow-up of the two prospective cohort studies, we documented 4,465 incident colorectal cancer cases, including 933 cases with available data on *F. nucleatum* and T cells in tumor tissue. We used covariate data of the 4,465 cases to adjust for selection bias in the 933 cases in multivariable analyses to conduct our primary hypothesis testing. *F. nucleatum* DNA was detected using a quantitative PCR assay in 128 (14%) of the 933 cases. **Table 1** shows clinical, pathological, and molecular features of colorectal cancer cases according to the amount of *F. nucleatum* DNA. Greater amounts of *F. nucleatum* DNA were associated with poor tumor differentiation, MSI-high status, CIMP-high status, BRAF mutation, higher tumor neoantigen loads, and higher exome-wide tumor mutational burden ($P < 0.005$; with the α level of 0.005) but not with *KRAS* or *PIK3CA* mutation.

Initial analyses using Spearman's correlation test on each of the T cell subset densities in tumor intraepithelial and stromal regions revealed that the densities of $CD3^+$ cells, $CD3^+CD4^+$ cells, and $CD3^+CD4^+CD45RO^+$ cells in tumor stromal areas were inversely correlated with the amount of *F. nucleatum* ($P < 0.005$ with the α level of 0.005) (**Table 1** and **Figure 1A**). In contrast, the amount of tissue *F. nucleatum* was not associated with intraepithelial densities of T cell subsets. Representative multiplex immunofluorescence and cell-phenotype images of *F. nucleatum* negative, low, and high cases are shown in **Figure 1B**.

In our primary hypothesis testing, we used a logistic regression analysis to assess the association of the amount of *F. nucleatum* DNA with the densities of T cell subsets which were selected by the initial analyses (**Table 2**, and **Supplementary Tables S1** and **S2**). In the multivariable analyses, the amount of *F. nucleatum* DNA in colorectal cancer tissue was inversely associated with densities of stromal $CD3^+$ cells ($P_{trend} = 0.0004$) and $CD3^+CD4^+CD45RO^+$ cells ($P_{trend} = 0.003$) with the α level of 0.005. For a unit increase in four ordinal categories of stromal $CD3^+$ cell density, multivariable odd ratios (ORs) were 0.51 [95% confidence interval (CI), 0.30-0.87] for *F. nucleatum*-low cases and 0.47 (95% CI, 0.28-0.79) for *F. nucleatum*-high cases, compared with *F. nucleatum*-negative cases. For a unit increase in four ordinal categories of stromal $CD3^+CD4^+CD45RO^+$ cell density, multivariable ORs were 0.67 (95% CI, 0.41-1.10) for *F. nucleatum*-low cases and 0.52 (95% CI, 0.32-0.85) for *F. nucleatum*-high cases, compared with *F. nucleatum*-negative cases. The amount of *F. nucleatum* in colorectal cancer tissue was not significantly associated with the density of $CD3^+CD4^+$ cells or $CD3^+CD4^+CD45RO^-$ cells (with the α level of 0.005).

As secondary analyses, we examined the statistical interaction between *F. nucleatum* and MSI status in relation to densities of stromal $CD3^+$ cells and $CD3^+CD4^+CD45RO^+$ cells. We did not observe a significant interaction between *F. nucleatum* and MSI status (**Table 3**).

Additional secondary analyses were performed using a subset of cases with available neoantigen loads or exome-wide tumor mutational burden data as measured by whole exome sequencing. Evaluation of the statistical interaction between *F. nucleatum* and neoantigen loads (or exome-wide tumor mutational burden) in relation to densities of stromal $CD3^+$ cells and $CD3^+CD4^+CD45RO^+$ cells did not identify a significant interaction between *F. nucleatum* and neoantigen loads (**Table 4**) or exome-wide tumor mutational burden (**Table 5**).

In exploratory analyses, we did not observe a statistically significant association between *F. nucleatum* DNA amount and any TAM subset in tumor intraepithelial or stromal regions ($P > 0.01$; with the α level of 0.005) (**Table 1** and **Supplementary Table S3**).

We further examined the association of *Bifidobacterium* genus with T cell subset densities and did not observe a significant association between *Bifidobacterium* genus and any T cell subset in intraepithelial or stromal regions ($P > 0.2$) (**Supplementary Table S4**).

Discussion

As colorectal cancer is a group of heterogenous tumors influenced by the microbiota and immune system, we conducted this study utilizing a molecular pathological epidemiology database (38) based on two the prospective cohort studies, to examine the relations between *F. nucleatum* and T cell infiltrates while controlling for confounders and selection bias. By employing a quantitative, multiplexed immunofluorescence assay. we found an inverse association of *F. nucleatum* with tumor stromal $CD3^+$ T cells, particularly stromal $CD3^+CD4^+CD45RO^+$ memory helper T cells that was independent of MSI status, neoantigen loads, and exome-wide tumor mutational burden. To our knowledge, our analysis is the first human population study to show the relationship between *F. nucleatum* amount and memory helper T cells in tumor stroma. Our findings not only aid the understanding of *F. nucleatum* associated immunosuppression but also underscore the importance of in-situ localization of specific T cell subsets in the colorectal cancer microenvironment.

The tumor immune microenvironment comprises transformed neoplastic cells, infiltrating immune cells, other stromal cells, and extracellular matrices. Recent advances in digital pathology have revealed the importance of both the characterization and localization of immune cells (10). Multiplex immunofluorescence allows detailed phenotyping of immune cells, which improves understanding of tumor-immune interactions (13). Mature T cells, expressing CD3, are largely comprised of $CD8^+$ T cells and $CD4^+$ helper T cells. Within these two major classes, naïve and memory T cells can be distinguished based on expression of CD45RO, and regulatory T cells can be identified by expression of the FOXP3 transcription factor (39). While T cells play a major role in the adaptive immune response against cancer, specific T cell subsets have

divergent functions. Tumor-infiltrating lymphocytes, specifically $CD8^+$ T cells, represent the cytotoxic arms of adaptive immune response and have been associated with better survival, while $CD4^+$ T cells (mostly in the helper T cell lineage) appear to enhance anti-tumor activity of cytotoxic T cells (40,41). Tumor stromal lymphocytes, which are generally more abundant than intraepithelial ones, have also been associated with favorable prognosis in colorectal cancer (42); however, different cell types such as naïve, memory, and regulatory T cells may have different implications. Our intriguing findings suggest the potential interplay between *F. nucleatum* and memory helper T cells in tumor stroma.

There is a growing body of evidence on the influential role of microbiota on cancer immunosurveillance and the modulation of immunotherapy responsiveness (43-46). *F. nucleatum* has emerged as a potentially oncogenic microorganism, which may drive inflammation-related carcinogenesis and recruit myeloid-derived suppressor cells (20). Experimental studies also have shown that *F. nucleatum* may inhibit T cell- and natural killer cell-mediated immune response against colorectal cancer through the immune cell receptor TIGIT (21). In accordance with these experimental lines of evidence, our findings support the immunosuppressive role of *F. nucleatum* in the human colorectal cancer microenvironment. Interestingly, despite the ability of *F. nucleatum* to adhere and invade into tumor epithelial cells (19,47), the densities of T cells within tumor epithelial regions were not correlated with *F. nucleatum* levels. Given that invasive *F. nucleatum* distribution appears highly heterogenous and focal in the colorectal cancer tissues in terms of gross tumor center versus invasive margin, as well as microscopic tumor epithelia versus stroma (48), *F. nucleatum* may interact with

stromal components including myeloid-derived suppressor cells, which inhibit T cell proliferation and induce T cell apoptosis (20). The amount of *F. nucleatum* in colorectal cancer has been associated with proximal tumor location, high-level MSI status, lower T cell infiltrates, and worse prognosis (18,49-51). Evidence also suggests that *F. nucleatum* may exert differential immunosuppressive or modulatory effects according to tumor MSI status (52). A better understanding of the interaction between *F. nucleatum* and specific immune cell phenotypes could have considerable implications on the development of therapeutic strategies that help overcome scarcity of T cell infiltration and increase the fraction of patients responding to immunotherapy.

We acknowledge limitations of this study. First, considering the cross-sectional nature of our study, we cannot exclude the possibility of reverse causation. Although it is possible that T cells may contribute in the elimination of *F. nucleatum*, our specific hypothesis was based on several lines of experimental evidence indicating that *F. nucleatum* suppresses the adaptive immune responses against colorectal cancer (21). Second, since our study was driven by a specific hypothesis, we focused on *F. nucleatum* in relation to T cells. Accumulating evidence suggests that various species of microbiota are involved in tumor development and anti-tumor immune response (1,2). Although we determined that there was no significant association between *Bifidobacterium* genus and T cell densities as an exploratory analysis, more comprehensive bacterial analyses such as metagenomic sequencing would help further characterize the relationship between tumor microbiota and the antitumor immune response. Third, we used the quantitative PCR assay for *F. nucleatum* in FFPE tissue specimens. Histopathology procedures and storage conditions may have influenced

the detection rates and quantification. Nonetheless, our previous validation study using the quantitative PCR assay showed both a good concordance in detection of *F. nucleatum* in paired FFPE and frozen tissue specimens as well as high linearity and reproducibility of *F. nucleatum* measurements in FFPE tissue specimens (18).

The current study has notable strengths, including the use of a molecular pathological epidemiology database derived from two U.S.-based large prospective cohort studies. Because no experimental model could recapitulate the complexity of human tumor immune microenvironment, which can be modified by various factors including genetic and epigenetic alterations, lifestyle and environmental exposures, the microbiota, and host factors (53-55), the importance of the integrated data analyses on microbial features, tumor molecular characteristics, clinicopathological findings, and immunological profiling cannot be overemphasized. Second, our analyses within the prospective cohort studies enabled us to use the IPW method and covariate data of all 4,465 incident colorectal cancer cases to control for selection bias due to tissue data availability. Third, we utilized multiplexed immunofluorescence assays to identify and quantify specific subsets of T cells and macrophages in archival tumor tissue. In contrast to commonly used immunohistochemistry, our assays enabled us to deeply subclassify immune cells and discover the link between *F. nucleatum* and memory helper T cells. Fourth, unlike common studies based on cases drawn from few hospitals, our study subjects were derived from over a hundred of hospitals located throughout the U.S., which increases the generalizability of our findings. Nevertheless, our findings need to be validated in independent studies.

In conclusion, this cross-sectional study utilizing the two U.S.-wide prospective cohort studies has shown an inverse association of *F. nucleatum* DNA in colorectal carcinoma tissue with tumor stromal densities of $CD3^+$ cell and $CD3^+CD4^+CD45RO^+$ cells. These findings provide a compelling rationale for further investigations into the interplay of the microbiota and T lymphocytes in colorectal carcinoma, potentially leading to novel strategies for cancer prevention and therapy.

Acknowledgments

We would like to thank the participants and staff of the Nurses' Health Study and the Health Professionals Follow-up Study for their valuable contributions as well as the following state cancer registries for their help: AL, AZ, AR, CA, CO, CT, DE, FL, GA, ID, IL, IN, IA, KY, LA, ME, MD, MA, MI, NE, NH, NJ, NY, NC, ND, OH, OK, OR, PA, RI, SC, TN, TX, VA, WA, WY. The authors assume full responsibility for analyses and interpretation of these data. This work was supported by U.S. National Institutes of Health (NIH) grants (P01 CA87969 to M.J. Stampfer; UM1 CA186107 to M.J. Stampfer; P01 CA55075 to W.C. Willett; UM1 CA167552 to W.C. Willett; U01 CA167552 to W.C. Willett and L.A. Mucci; P50 CA127003 to C.S.F.; R01 CA118553 to C.S.F.; R01 CA169141 to C.S.F.; R01 CA137178 to A.T.C.; K24 DK098311 to A.T.C.; R35 CA197735 to S.O.; R01 CA151993 to S.O.; K07 CA190673 to R.N.; K07 CA188126 to X.Z.; R01 CA225655 to J.K.L.; R01 CA248857 to S.O., U.P., and A.I.P.; P50 CA101942 (to G.J.F.); by Cancer Research UK's Grand Challenge Award (UK C10674/A27140 to K.N., W.S.G., M.G., C.H., and S.O.); by Nodal Award (2016-02) from the Dana-Farber Harvard Cancer Center (to S.O. and G.J.F.); by a Stand Up to Cancer Colorectal Cancer Dream Team Translational Research Grant (SU2C-AACR-DT22-17 to C.S.F. and M.G.), and by grants from the Project P Fund, The Friends of the Dana-Farber Cancer Institute, Bennett Family Fund, and the Entertainment Industry Foundation through National Colorectal Cancer Research Alliance and SU2C. Stand Up to Cancer is a division of the Entertainment Industry Foundation. The indicated SU2C research grant is administered by the American Association for Cancer Research, the scientific partner of SU2C. J.B. was supported by a grant from the Australia Awards-Endeavour Scholarships and Fellowships Program. K.H. was supported by fellowship grants from the Uehara Memorial Foundation and the Mitsukoshi Health and Welfare Foundation. K.A. was supported by a grant from Overseas Research Fellowship (JP2018-60083) from Japan Society for the Promotion of Science. K.F. was supported by a fellowship grant from the Uehara Memorial Foundation. S.A.V. was supported by Finnish Cultural

Foundation and Orion Research Foundation. J.A.M. research is supported by the Douglas Gray Woodruff Chair fund, the Guo Shu Shi Fund, Anonymous Family Fund for Innovations in Colorectal Cancer, P fund and the George Stone Family Foundation. M.G. is supported by an ASCO Conquer Cancer Foundation Career Development Award. A.T.C. is a Stuart and Suzanne Steele MGH Research Scholar. The content is solely the responsibility of the authors and does not necessarily represent the official views of NIH. The funders had no role in study design, data collection and analysis, decision to publish, or preparation of the manuscript.

References

1. Rajpoot M, Sharma AK, Sharma A, Gupta GK. Understanding the microbiome: Emerging biomarkers for exploiting the microbiota for personalized medicine against cancer. Semin Cancer Biol **2018**;52(Pt 1):1-8 doi 10.1016/j.semcancer.2018.02.003.

2. Inamura K. Gut microbiota contributes towards immunomodulation against cancer: New frontiers in precision cancer therapeutics. Semin Cancer Biol **2020** doi 10.1016/j.semcancer.2020.06.006.

3. Chen B, Du G, Guo J, Zhang Y. Bugs, drugs, and cancer: can the microbiome be a potential therapeutic target for cancer management? Drug Discov Today **2019**;24(4):1000-9 doi 10.1016/j.drudis.2019.02.009.

4. El Bairi K, Jabi R, Trapani D, Boutallaka H, Ouled Amar Bencheikh B, Bouziane M*, et al.* Can the microbiota predict response to systemic cancer therapy, surgical outcomes, and survival? The answer is in the gut. Expert Rev Clin Pharmacol **2020**;13(4):403-21 doi 10.1080/17512433.2020.1758063.

5. Kamal Y, Schmit SL, Frost HR, Amos CI. The tumor microenvironment of colorectal cancer metastases: opportunities in cancer immunotherapy. Immunotherapy **2020**;12(14):1083-100 doi 10.2217/imt-2020-0026.

6. Kather JN, Halama N. Harnessing the innate immune system and local immunological microenvironment to treat colorectal cancer. Br J Cancer **2019**;120(9):871-82 doi 10.1038/s41416-019-0441-6.

7. Ribas A, Wolchok JD. Cancer immunotherapy using checkpoint blockade. Science **2018**;359(6382):1350-5 doi 10.1126/science.aar4060.

8. Le DT, Uram JN, Wang H, Bartlett BR, Kemberling H, Eyring AD*, et al.* PD-1 Blockade in Tumors with Mismatch-Repair Deficiency. N Engl J Med **2015**;372(26):2509-20 doi 10.1056/NEJMoa1500596.

9. Ciardiello D, Vitiello PP, Cardone C, Martini G, Troiani T, Martinelli E*, et al.* Immunotherapy of colorectal cancer: Challenges for therapeutic efficacy. Cancer Treat Rev **2019**;76:22-32 doi 10.1016/j.ctrv.2019.04.003.

10. Pages F, Mlecnik B, Marliot F, Bindea G, Ou FS, Bifulco C*, et al.* International validation of the consensus Immunoscore for the classification of colon cancer: a prognostic and accuracy study. Lancet **2018**;391(10135):2128-39 doi 10.1016/s0140-6736(18)30789-x.

11. Nosho K, Baba Y, Tanaka N, Shima K, Hayashi M, Meyerhardt JA*, et al.* Tumour-infiltrating T-cell subsets, molecular changes in colorectal cancer, and

prognosis: cohort study and literature review. J Pathol **2010**;222(4):350-66 doi 10.1002/path.2774.

12. Marisa L, Svrcek M, Collura A, Becht E, Cervera P, Wanherdrick K*, et al.* The Balance Between Cytotoxic T-cell Lymphocytes and Immune Checkpoint Expression in the Prognosis of Colon Tumors. J Natl Cancer Inst **2018**;110(1) doi 10.1093/jnci/djx136.

13. Gartrell RD, Marks DK, Hart TD, Li G, Davari DR, Wu A*, et al.* Quantitative Analysis of Immune Infiltrates in Primary Melanoma. Cancer Immunol Res **2018**;6(4):481-93 doi 10.1158/2326-6066.Cir-17-0360.

14. Brennan CA, Garrett WS. Fusobacterium nucleatum - symbiont, opportunist and oncobacterium. Nat Rev Microbiol **2019**;17(3):156-66 doi 10.1038/s41579-018-0129-6.

15. Luo K, Zhang Y, Xv C, Ji J, Lou G, Guo X*, et al.* Fusobacterium nucleatum, the communication with colorectal cancer. Biomed Pharmacother **2019**;116:108988 doi 10.1016/j.biopha.2019.108988.

16. Kostic AD, Gevers D, Pedamallu CS, Michaud M, Duke F, Earl AM*, et al.* Genomic analysis identifies association of Fusobacterium with colorectal carcinoma. Genome Res **2012**;22(2):292-8 doi 10.1101/gr.126573.111.

17. Castellarin M, Warren RL, Freeman JD, Dreolini L, Krzywinski M, Strauss J*, et al.* Fusobacterium nucleatum infection is prevalent in human colorectal carcinoma. Genome Res **2012**;22(2):299-306 doi 10.1101/gr.126516.111.

18. Mima K, Sukawa Y, Nishihara R, Qian ZR, Yamauchi M, Inamura K*, et al.* Fusobacterium nucleatum and T Cells in Colorectal Carcinoma. JAMA Oncol **2015**;1(5):653-61 doi 10.1001/jamaoncol.2015.1377.

19. Rubinstein MR, Wang X, Liu W, Hao Y, Cai G, Han YW. Fusobacterium nucleatum promotes colorectal carcinogenesis by modulating E-cadherin/beta-catenin signaling via its FadA adhesin. Cell Host Microbe **2013**;14(2):195-206 doi 10.1016/j.chom.2013.07.012.

20. Kostic AD, Chun E, Robertson L, Glickman JN, Gallini CA, Michaud M*, et al.* Fusobacterium nucleatum potentiates intestinal tumorigenesis and modulates the tumor-immune microenvironment. Cell Host Microbe **2013**;14(2):207-15 doi 10.1016/j.chom.2013.07.007.

21. Gur C, Ibrahim Y, Isaacson B, Yamin R, Abed J, Gamliel M*, et al.* Binding of the Fap2 protein of Fusobacterium nucleatum to human inhibitory receptor TIGIT protects tumors from immune cell attack. Immunity **2015**;42(2):344-55 doi 10.1016/j.immuni.2015.01.010.

22. Mehta RS, Nishihara R, Cao Y, Song M, Mima K, Qian ZR*, et al.* Association of Dietary Patterns With Risk of Colorectal Cancer Subtypes Classified by Fusobacterium nucleatum in Tumor Tissue. JAMA Oncol **2017**;3(7):921-7 doi 10.1001/jamaoncol.2016.6374.

23. Liao X, Lochhead P, Nishihara R, Morikawa T, Kuchiba A, Yamauchi M*, et al.* Aspirin use, tumor PIK3CA mutation, and colorectal-cancer survival. N Engl J Med **2012**;367(17):1596-606 doi 10.1056/NEJMoa1207756.

24. Haruki K, Kosumi K, Hamada T, Twombly TS, Väyrynen JP, Kim SA*, et al.* Association of autophagy status with amount of Fusobacterium nucleatum in colorectal cancer. J Pathol **2020**;250(4):397-408 doi 10.1002/path.5381.

25. Yamauchi M, Morikawa T, Kuchiba A, Imamura Y, Qian ZR, Nishihara R*, et al.* Assessment of colorectal cancer molecular features along bowel subsites challenges the conception of distinct dichotomy of proximal versus distal colorectum. Gut **2012**;61(6):847-54 doi 10.1136/gutjnl-2011-300865.

26. Chan AT, Ogino S, Fuchs CS. Aspirin and the risk of colorectal cancer in relation to the expression of COX-2. N Engl J Med **2007**;356(21):2131-42 doi 10.1056/NEJMoa067208.

27. Fujiyoshi K, Väyrynen JP, Borowsky J, Papke DJ, Jr., Arima K, Haruki K*, et al.* Tumour budding, poorly differentiated clusters, and T-cell response in colorectal cancer. EBioMedicine **2020**;57:102860 doi 10.1016/j.ebiom.2020.102860.

28. Lau MC, Borowsky J, Väyrynen JP, Haruki K, Zhao M, Costa AD*, et al.* Tumor-Immune Partitioning and Clustering (TIPC) algorithm reveals distinct signatures of tumor-immune cell interactions within the tumor microenvironment. bioRxiv **2020**:2020.05.29.111542 doi 10.1101/2020.05.29.111542.

29. Fujiyoshi K, Bruford EA, Mroz P, Sims CL, O'Leary TJ, Lo AWI*, et al.* Opinion: Standardizing gene product nomenclature-a call to action. Proc Natl Acad Sci U S A **2021**;118(3) doi 10.1073/pnas.2025207118.

30. Väyrynen JP, Haruki K, Lau MC, Väyrynen SA, Zhong R, Dias Costa A*, et al.* The Prognostic Role of Macrophage Polarization in the Colorectal Cancer Microenvironment. Cancer Immunol Res **2020** doi 10.1158/2326-6066.Cir-20-0527.

31. Kosumi K, Hamada T, Koh H, Borowsky J, Bullman S, Twombly TS*, et al.* The Amount of Bifidobacterium Genus in Colorectal Carcinoma Tissue in Relation to Tumor Characteristics and Clinical Outcome. Am J Pathol **2018**;188(12):2839-52 doi 10.1016/j.ajpath.2018.08.015.

32. Nosho K, Irahara N, Shima K, Kure S, Kirkner GJ, Schernhammer ES*, et al.* Comprehensive biostatistical analysis of CpG island methylator phenotype in

colorectal cancer using a large population-based sample. PLoS One **2008**;3(11):e3698 doi 10.1371/journal.pone.0003698.

33. Imamura Y, Lochhead P, Yamauchi M, Kuchiba A, Qian ZR, Liao X*, et al.* Analyses of clinicopathological, molecular, and prognostic associations of KRAS codon 61 and codon 146 mutations in colorectal cancer: cohort study and literature review. Mol Cancer **2014**;13:135 doi 10.1186/1476-4598-13-135.

34. Giannakis M, Mu XJ, Shukla SA, Qian ZR, Cohen O, Nishihara R*, et al.* Genomic Correlates of Immune-Cell Infiltrates in Colorectal Carcinoma. Cell Rep **2016**;15(4):857-65 doi 10.1016/j.celrep.2016.03.075.

35. Nielsen M, Andreatta M. NetMHCpan-3.0; improved prediction of binding to MHC class I molecules integrating information from multiple receptor and peptide length datasets. Genome Med **2016**;8(1):33 doi 10.1186/s13073-016-0288-x.

36. Benjamin DJ, Berger JO, Johannesson M, Nosek BA, Wagenmakers EJ, Berk R*, et al.* Redefine statistical significance. Nat Hum Behav **2018**;2(1):6-10 doi 10.1038/s41562-017-0189-z.

37. Liu L, Nevo D, Nishihara R, Cao Y, Song M, Twombly TS*, et al.* Utility of inverse probability weighting in molecular pathological epidemiology. Eur J Epidemiol **2018**;33(4):381-92 doi 10.1007/s10654-017-0346-8.

38. Akimoto N, Ugai T, Zhong R, Hamada T, Fujiyoshi K, Giannakis M*, et al.* Rising incidence of early-onset colorectal cancer - a call to action. Nat Rev Clin Oncol **2020** doi 10.1038/s41571-020-00445-1.

39. Golubovskaya V, Wu L. Different Subsets of T Cells, Memory, Effector Functions, and CAR-T Immunotherapy. Cancers (Basel) **2016**;8(3) doi 10.3390/cancers8030036.

40. Bou Nasser Eddine F, Ramia E, Tosi G, Forlani G, Accolla RS. Tumor Immunology meets...Immunology: Modified cancer cells as professional APC for priming naive tumor-specific CD4+ T cells. Oncoimmunology **2017**;6(11):e1356149 doi 10.1080/2162402x.2017.1356149.

41. Aspeslagh S, Morel D, Soria JC, Postel-Vinay S. Epigenetic modifiers as new immunomodulatory therapies in solid tumours. Ann Oncol **2018**;29(4):812-24 doi 10.1093/annonc/mdy050.

42. Haruki K, Kosumi K, Li P, Arima K, Vayrynen JP, Lau MC*, et al.* An integrated analysis of lymphocytic reaction, tumour molecular characteristics and patient survival in colorectal cancer. Br J Cancer **2020**;122(9):1367-77 doi 10.1038/s41416-020-0780-3.

43. Sears CL, Pardoll DM. The intestinal microbiome influences checkpoint blockade. Nat Med **2018**;24(3):254-5 doi 10.1038/nm.4511.

44. Gopalakrishnan V, Helmink BA, Spencer CN, Reuben A, Wargo JA. The Influence of the Gut Microbiome on Cancer, Immunity, and Cancer Immunotherapy. Cancer Cell **2018**;33(4):570-80 doi 10.1016/j.ccell.2018.03.015.

45. Zitvogel L, Pietrocola F, Kroemer G. Nutrition, inflammation and cancer. Nat Immunol **2017**;18(8):843-50 doi 10.1038/ni.3754.

46. Murphy CL, O'Toole PW, Shanahan F. The Gut Microbiota in Causation, Detection, and Treatment of Cancer. Am J Gastroenterol **2019**;114(7):1036-42 doi 10.14309/ajg.0000000000000075.

47. Abed J, Emgard JE, Zamir G, Faroja M, Almogy G, Grenov A*, et al.* Fap2 Mediates Fusobacterium nucleatum Colorectal Adenocarcinoma Enrichment by Binding to Tumor-Expressed Gal-GalNAc. Cell Host Microbe **2016**;20(2):215-25 doi 10.1016/j.chom.2016.07.006.

48. Bullman S, Pedamallu CS, Sicinska E, Clancy TE, Zhang X, Cai D*, et al.* Analysis of Fusobacterium persistence and antibiotic response in colorectal cancer. Science **2017**;358(6369):1443-8 doi 10.1126/science.aal5240.

49. Mima K, Nishihara R, Qian ZR, Cao Y, Sukawa Y, Nowak JA*, et al.* Fusobacterium nucleatum in colorectal carcinoma tissue and patient prognosis. Gut **2016**;65(12):1973-80 doi 10.1136/gutjnl-2015-310101.

50. Mima K, Cao Y, Chan AT, Qian ZR, Nowak JA, Masugi Y*, et al.* Fusobacterium nucleatum in Colorectal Carcinoma Tissue According to Tumor Location. Clin Transl Gastroenterol **2016**;7(11):e200 doi 10.1038/ctg.2016.53.

51. Nosho K, Sukawa Y, Adachi Y, Ito M, Mitsuhashi K, Kurihara H*, et al.* Association of Fusobacterium nucleatum with immunity and molecular alterations in colorectal cancer. World J Gastroenterol **2016**;22(2):557-66 doi 10.3748/wjg.v22.i2.557.

52. Hamada T, Zhang X, Mima K, Bullman S, Sukawa Y, Nowak JA*, et al.* Fusobacterium nucleatum in Colorectal Cancer Relates to Immune Response Differentially by Tumor Microsatellite Instability Status. Cancer Immunol Res **2018**;6(11):1327-36 doi 10.1158/2326-6066.Cir-18-0174.

53. Ogino S, Chan AT, Fuchs CS, Giovannucci E. Molecular pathological epidemiology of colorectal neoplasia: an emerging transdisciplinary and interdisciplinary field. Gut **2011**;60(3):397-411 doi 10.1136/gut.2010.217182.

54. Ogino S, Nowak JA, Hamada T, Milner DA, Jr., Nishihara R. Insights into Pathogenic Interactions Among Environment, Host, and Tumor at the Crossroads of Molecular Pathology and Epidemiology. Annu Rev Pathol **2019**;14:83-103 doi 10.1146/annurev-pathmechdis-012418-012818.

55. Wang ST, Cui WQ, Pan D, Jiang M, Chang B, Sang LX. Tea polyphenols and their chemopreventive and therapeutic effects on colorectal cancer. World J Gastroenterol **2020**;26(6):562-97 doi 10.3748/wjg.v26.i6.562.

Author Manuscript Published OnlineFirst on February 25, 2021; DOI: 10.1158/1078-0432.CCR-20-4009
Author manuscripts have been peer reviewed and accepted for publication but have not yet been edited.

Table 1. Clinical, Pathological, and Molecular Characteristics of Colorectal Cancer Cases According to *Fusobacterium nucleatum* DNA Amount in Tumor Tissue

Characteristic*	All cases (N = 933)	*F. nucleatum* DNA in tumor tissue: Negative (N = 805)	Low (N = 64)	High (N = 64)	*P* value†
Sex					0.61
Female (NHS)	513 (55%)	439 (55%)	35 (55%)	39 (61%)	
Male (HPFS)	420 (45%)	366 (45%)	29 (45%)	25 (39%)	
Mean age ± SD (years)	69.1 ± 8.8	69.0 ± 8.9	70.6 ± 8.6	68.9 ± 8.0	0.37
Year of diagnosis					0.13
1995 or before	300 (32%)	268 (33%)	13 (20%)	19 (30%)	
1996-2000	307 (33%)	264 (33%)	20 (31%)	23 (36%)	
2001-2012	326 (35%)	273 (34%)	31 (48%)	22 (34%)	
Family history of colorectal cancer in first-degree relative(s)					0.69
Absent	730 (79%)	627 (78%)	51 (81%)	52 (83%)	
Present	195 (21%)	172 (22%)	12 (19%)	11 (17%)	
Tumor location					0.084
Cecum	166 (18%)	135 (18%)	16 (25%)	15 (23%)	
Ascending to transverse colon	300 (32%)	253 (32%)	23 (36%)	24 (38%)	
Descending to sigmoid colon	276 (30%)	251 (30%)	10 (16%)	15 (23%)	
Rectum	187 (20%)	162 (20%)	15 (23%)	10 (16%)	
Tumor differentiation					< 0.0001
Well to moderate	846 (91%)	745 (93%)	52 (83%)	49 (77%)	
Poor	86 (9.2%)	60 (7.5%)	11 (17%)	15 (23%)	
AJCC disease stage					0.090
I	201 (23%)	184 (25%)	8 (14%)	9 (15%)	
II	284 (33%)	235 (32%)	22 (38%)	27 (44%)	
III	251 (29%)	214 (29%)	22 (38%)	15 (25%)	
IV	127 (15%)	111 (15%)	6 (10%)	10 (16%)	
MSI status					< 0.0001
Non-MSI-high	750 (83%)	669 (86%)	42 (69%)	39 (61%)	
MSI-high	156 (17%)	112 (14%)	19 (31%)	25 (39%)	
CIMP status					< 0.0001
Low/negative	708 (82%)	627 (84%)	46 (78%)	35 (58%)	
High	160 (18%)	122 (16%)	13 (22%)	25 (42%)	
Mean LINE-1 methylation level ± SD (%)	62.5 ± 9.6	62.2 ± 9.6	63.0 ± 9.3	64.8 ± 9.9	0.099
KRAS mutation					0.33
Wild-type	536 (59%)	466 (59%)	30 (51%)	40 (63%)	
Mutant	370 (41%)	318 (41%)	29 (49%)	23 (37%)	
BRAF mutation					0.0009
Wild-type	776 (85%)	680 (86%)	52 (85%)	44 (69%)	
Mutant	138 (15%)	109 (14%)	9 (15%)	20 (31%)	

Author Manuscript Published OnlineFirst on February 25, 2021; DOI: 10.1158/1078-0432.CCR-20-4009
Author manuscripts have been peer reviewed and accepted for publication but have not yet been edited.

PIK3CA mutation					0.95
Wild-type	715 (84%)	618 (84%)	46 (82%)	51 (84%)	
Mutant	139 (16%)	119 (16%)	10 (18%)	10 (16%)	
Neoantigen loads					0.0002
Q1 (lowest)	107 (25%)	94 (26%)	6 (19%)	7 (23%)	
Q2	105 (25%)	91 (25%)	10 (31%)	4 (13%)	
Q3	106 (25%)	100 (28%)	4 (13%)	2 (6.7%)	
Q4 (highest)	106 (25%)	77 (21%)	12 (37%)	17 (57%)	
Exome wide tumor mutation burden					0.001
Q1 (lowest)	107 (25%)	95 (26%)	6 (19%)	6 (20%)	
Q2	106 (25%)	95 (26%)	7 (22%)	4 (13%)	
Q3	105 (25%)	95 (26%)	7 (22%)	3 (10%)	
Q4 (highest)	106 (25%)	77 (21%)	12 (38%)	17 (57%)	
Median stromal $CD3^+$ cell density (IQR) ($cells/mm^2$)	145 (22-493)	162 (26-538)	94 (6.8-302)	71 (6.9-238)	0.0002‡
Median stromal $CD3^+CD4^+$ cell density (IQR) ($cells/mm^2$)	76 (3.8-361)	84 (4.9-392)	44 (0-207)	37 (0-164)	0.0007‡
Median stromal $CD3^+CD8^+$ cell density (IQR) ($cells/mm^2$)	10 (0-54)	10 (0-56)	11 (0-56)	9.3 (0-34)	0.69‡
Median stromal $CD3^+CD4^+CD45RO^+$ cell density (IQR) ($cells/mm^2$)	57 (0-287)	67 (2.9-329)	33 (0-162)	24 (0-134)	0.0006‡
Median stromal $CD3^+CD4^+CD45RO^-$ cell density (IQR) ($cells/mm^2$)	7.2 (0-48)	7.7 (0-51)	0 (0-38)	4.2 (0-26)	0.034‡
Median stromal overall macrophage density (IQR) ($cells/mm^2$)	871 (489-1428)	859 (479-1399)	966 (579-1667)	894 (609-1477)	0.33‡
Median stromal M1-like macrophage density (IQR) ($cells/mm^2$)	175 (65-398)	170 (62-379)	202 (68-548)	192 (85-452)	0.14‡
Median stromal M2-like macrophage density (IQR) ($cells/mm^2$)	192 (69-429)	192 (69-435)	191 (69-435)	196 (63-431)	0.33‡
Bifidobacterium genus DNA in tumor tissue					
Negative	631 (71%)	556 (72%)	38 (64%)	37 (62%)	0.094
Low	128 (14%)	104 (14%)	9 (15%)	15 (25%)	
High	128 (14%)	108 (14%)	12 (20%)	8 (13%)	

* Percentage indicates the proportion of patients with a specific clinical, pathologic, or molecular characteristic among all patients or in strata of *F. nucleatum* DNA amount.
† To compare categorical data between subgroups classified by *F. nucleatum* DNA amount, the chi-square test was performed, unless otherwise noted. To compare continuous variables, an analysis of variance was performed.
‡ To assess associations between *F. nucleatum* DNA amount (continuous) and densities of T cell subsets and macrophage (continuous), the Spearman's correlation test was performed.

Abbreviations: AJCC, American Joint Committee on Cancer; CIMP, CpG island methylator phenotype; HPFS, Health Professionals Follow-up Study; IQR, interquartile range; LINE-1, long-interspersed nucleotide element-1; MSI, microsatellite instability; NHS, Nurses' Health Study; SD, standard deviation.

Table 2. Inverse Probability Weighting (IPW)-Adjusted Logistic Regression Analysis to Assess the Associations of *Fusobacterium nucleatum* (Predictor) with T Cell Density (Outcome)

	Univariable OR (95% CI)*	Multivariable OR (95% CI)*,†
Model for stromal $CD3^+$ cell density (as an ordinal outcome variable)		
Amount of *F. nucleatum* DNA		
Negative	1 (referent)	1 (referent)
Low	0.54 (0.33-0.91)	0.51 (0.30-0.87)
High	0.51 (0.30-0.84)	0.47 (0.28-0.79)
P_{trend}‡	0.001	0.0004
Model for stromal $CD3^+CD4^+$ cell density (as a binary outcome variable)		
Amount of *F. nucleatum* DNA		
Negative	1 (referent)	1 (referent)
Low	0.86 (0.49-1.48)	0.80 (0.46-1.39)
High	0.52 (0.29-0.91)	0.50 (0.28-0.89)
P_{trend}§	0.023	0.015
Model for stromal $CD3^+CD4^+CD45RO^+$ cell density (as an ordinal outcome variable)		
Amount of *F. nucleatum* DNA		
Negative	1 (referent)	1 (referent)
Low	0.66 (0.40-1.09)	0.67 (0.41-1.10)
High	0.53 (0.33-0.85)	0.52 (0.32-0.85)
P_{trend}‡	0.003	0.003
Model for stromal $CD3^+CD4^+CD45RO^-$ cell density (as an ordinal outcome variable)		
Amount of *F. nucleatum* DNA		
Negative	1 (referent)	1 (referent)
Low	0.73 (0.43-1.25)	0.74 (0.43-1.28)
High	0.75 (0.47-1.17)	0.75 (0.47-1.17)
P_{trend}‡	0.12	0.13

* IPW was applied to reduce a bias due to the availability of tumor tissue after cancer diagnosis (see "Statistical Analysis" subsection for details).

† The multivariable ordinal logistic regression model initially included age, sex, year of diagnosis, family history of colorectal cancer, tumor location, microsatellite instability, CpG island methylator phenotype, long-interspersed nucleotide element-1 methylation level, and *KRAS*, *BRAF*, and *PIK3CA* mutation status. A backward elimination with a threshold *P* of 0.20 was used to select variables for the final model. The variables which remained in the final models are shown in Supplementary Table S2.

‡ P_{trend} was calculated by the linear trend across the ordinal categories of *F. nucleatum* DNA amount (negative, low, and high, as an ordinal predictor variable) in the IPW-adjusted ordinal logistic regression model for the densities of T cells (4 ordinal categories, as an ordinal outcome variable).

§ To avoid violation of the proportional odds assumption, the density of $CD3^+CD4^+$ cell was dichotomized at the median value of subset. P_{trend} was calculated by the linear trend across the ordinal categories of *F. nucleatum* DNA amount (negative, low, and high, as an ordinal predictor variable) in the IPW-adjusted logistic regression model for the density of $CD3^+CD4^+$ cell (binary categories, as an outcome variable).

Abbreviations: CI, confidence interval; IPW, inverse probability weighting; OR, odds ratio.

Table 3. Inverse Probability Weighting (IPW)-Adjusted Logistic Regression Analysis to Assess the Associations of *Fusobacterium nucleatum* (Predictor) with T Cell Density (Outcome) in Strata of MSI Status

N = 906	Univariable OR (95% CI)*	Multivariable OR (95% CI)*,†
Model for stromal $CD3^+$ cell density‡ (as a binary outcome variable)		
Non-MSI-high		
Amount of *F. nucleatum* DNA		
Negative	1 (referent)	1 (referent)
Low	0.55 (0.27-1.11)	0.56 (0.28-1.15)
High	0.36 (0.16-0.79)	0.36 (0.16-0.80)
MSI-high		
Amount of *F. nucleatum* DNA		
Negative	1 (referent)	1 (referent)
Low	0.60 (0.21-1.68)	0.58 (0.20-1.66)
High	0.52 (0.21-1.31)	0.58 (0.23-1.46)
$P_{interaction}$§	0.53	0.47
Model for stromal $CD3^+CD4^+CD45RO^+$ cell density‡ (as a binary outcome variable)		
Non-MSI-high		
Amount of *F. nucleatum* DNA		
Negative	1 (referent)	1 (referent)
Low	0.56 (0.28-1.12)	0.55 (0.28-1.11)
High	0.43 (0.20-0.91)	0.42 (0.20-0.89)
MSI-high		
Amount of *F. nucleatum* DNA		
Negative	1 (referent)	1 (referent)
Low	0.76 (0.27-2.14)	0.72 (0.25-2.08)
High	0.57 (0.23-1.45)	0.62 (0.25-1.54)
$P_{interaction}$§	0.52	0.46

* IPW was applied to reduce a bias due to the availability of tumor tissue after cancer diagnosis (see "Statistical Analysis" subsection for details).
† The multivariable logistic regression model initially included age, sex, year of diagnosis, family history of colorectal cancer, tumor location, CpG island methylator phenotype, long-interspersed nucleotide element-1 methylation level, and *KRAS*, *BRAF*, and *PIK3CA* mutation status. A backward elimination with a threshold *P* of 0.20 was used to select variables for the final model.
‡ To avoid violation of the proportional odds assumption, the densities of T cells were dichotomized at the median value of each subset.
§ $P_{interaction}$ (two-sided) was calculated using the Wald test for the cross product of *F. nucleatum* DNA amount (negative, low, and high, as an ordinal predictor variable) and MSI status (high vs. non-high) in the IPW-adjusted logistic regression model.
Abbreviations: CI, confidence interval; IPW, inverse probability weighting; OR, odds ratio.

Table 4. Inverse Probability Weighting (IPW)-Adjusted Logistic Regression Analysis to Assess the Associations of *Fusobacterium nucleatum* (Predictor) with T Cell Density (Outcome) in Strata of Tumor Neoantigen Loads

N = 424	Univariable OR (95% CI)*	Multivariable OR (95% CI)*,†
Model for stromal $CD3^+$ cell density‡ (as an outcome variable)		
Neoantigen-low		
Amount of *F. nucleatum* DNA		
Negative	1 (referent)	1 (referent)
Low	0.86 (0.26-2.80)	0.94 (0.28-3.13)
High	0.50 (0.12-2.18)	0.47 (0.10-2.23)
Neoantigen-high		
Amount of *F. nucleatum* DNA		
Negative	1 (referent)	1 (referent)
Low	0.49 (0.16-1.49)	0.51 (0.17-1.55)
High	0.71 (0.27-1.90)	0.80 (0.29-2.25)
$P_{interaction}$§	0.71	0.85
Model for stromal $CD3^+CD4^+CD45RO^+$ cell density‡ (as an outcome variable)		
Neoantigen-low		
Amount of *F. nucleatum* DNA		
Negative	1 (referent)	1 (referent)
Low	0.84 (0.26-2.73)	0.90 (0.27-2.98)
High	0.49 (0.11-2.12)	0.49 (0.11-2.13)
Neoantigen-high		
Amount of *F. nucleatum* DNA		
Negative	1 (referent)	1 (referent)
Low	0.51 (0.17-1.58)	0.53 (0.18-1.60)
High	0.74 (0.28-1.98)	0.89 (0.32-2.50)
$P_{interaction}$§	0.88	0.99

* IPW was applied to reduce a bias due to the availability of tumor tissue after cancer diagnosis (see "Statistical Analysis" subsection for details).
† The multivariable logistic regression model initially included age, sex, year of diagnosis, family history of colorectal cancer, tumor location, microsatellite instability, CpG island methylator phenotype, long-interspersed nucleotide element-1 methylation level, and *KRAS*, *BRAF*, and *PIK3CA* mutation status. A backward elimination with a threshold *P* of 0.20 was used to select variables for the final model.
‡ To avoid violation of the proportional odds assumption, the densities of T cells were dichotomized at the median value of each subset.
§ $P_{interaction}$ (two-sided) was calculated using the Wald test for the cross product of *F. nucleatum* DNA amount (negative, low, and high, as an ordinal predictor variable) and neoantigen loads [high (Q3-4) vs. low (Q1-2)] in the IPW-adjusted logistic regression model.
Abbreviations: CI, confidence interval; IPW, inverse probability weighting; OR, odds ratio.

Author Manuscript Published OnlineFirst on February 25, 2021; DOI: 10.1158/1078-0432.CCR-20-4009
Author manuscripts have been peer reviewed and accepted for publication but have not yet been edited.

Table 5. Inverse Probability Weighting (IPW)-Adjusted Logistic Regression Analysis to Assess the Associations of *Fusobacterium nucleatum* (Predictor) with T Cell Density (Outcome) in Strata of Exome-wide Tumor Mutational Burden

N = 424	Univariable OR (95% CI)*	Multivariable OR (95% CI)*,†
Model for stromal $CD3^+$ cell density‡ (as an outcome variable)		
Exome-wide tumor mutational burden-low		
Amount of *F. nucleatum* DNA		
Negative	1 (referent)	1 (referent)
Low	1.08 (0.32-3.64)	1.07 (0.30-3.76)
High	0.48 (0.11-2.07)	0.43 (0.09-2.09)
Exome-wide tumor mutational burden-high		
Amount of *F. nucleatum* DNA		
Negative	1 (referent)	1 (referent)
Low	0.42 (0.15-1.18)	0.47 (0.17-1.33)
High	0.68 (0.26-1.80)	0.75 (0.28-2.06)
$P_{interaction}$§	0.68	0.77
Model for stromal $CD3^+CD4^+CD45RO^+$ cell density‡ (as an outcome variable)		
Exome-wide tumor mutational burden-low		
Amount of *F. nucleatum* DNA		
Negative	1 (referent)	1 (referent)
Low	1.15 (0.34-3.87)	1.15 (0.34-3.97)
High	0.51 (0.12-2.20)	0.50 (0.12-2.19)
Exome-wide tumor mutational burden-high		
Amount of *F. nucleatum* DNA		
Negative	1 (referent)	1 (referent)
Low	0.41 (0.14-1.14)	0.43 (0.15-1.22)
High	0.65 (0.25-1.71)	0.78 (0.29-2.15)
$P_{interaction}$§	0.71	0.82

* IPW was applied to reduce a bias due to the availability of tumor tissue after cancer diagnosis (see "Statistical Analysis" subsection for details).
† The multivariable logistic regression model initially included age, sex, year of diagnosis, family history of colorectal cancer, tumor location, microsatellite instability, CpG island methylator phenotype, long-interspersed nucleotide element-1 methylation level, and *KRAS*, *BRAF*, and *PIK3CA* mutation status. A backward elimination with a threshold *P* of 0.20 was used to select variables for the final model.
‡ To avoid violation of the proportional odds assumption, the densities of T cells were dichotomized at the median value of each subset.
§ $P_{interaction}$ (two-sided) was calculated using the Wald test for the cross product of *F. nucleatum* DNA amount (negative, low, and high, as an ordinal predictor variable) and exome-wide tumor mutational burden [high (Q3-4) vs. low (Q1-2)] in the IPW-adjusted logistic regression model.
Abbreviations: CI, confidence interval; IPW, inverse probability weighting; OR, odds ratio.

Figure Legend

Figure 1. Relationships between *Fusobacterium nucleatum* and T cell subsets in the colorectal cancer microenvironment. (A) Correlation between *Fusobacterium nucleatum* DNA amount in tumor tissue and density of T cell subsets in tumor intraepithelial and stromal regions. (B) Multiplex Immunofluorescence and cell-phenotype images of representative *Fusobacterium nucleatum* negative, low, and high case.

Figure 1

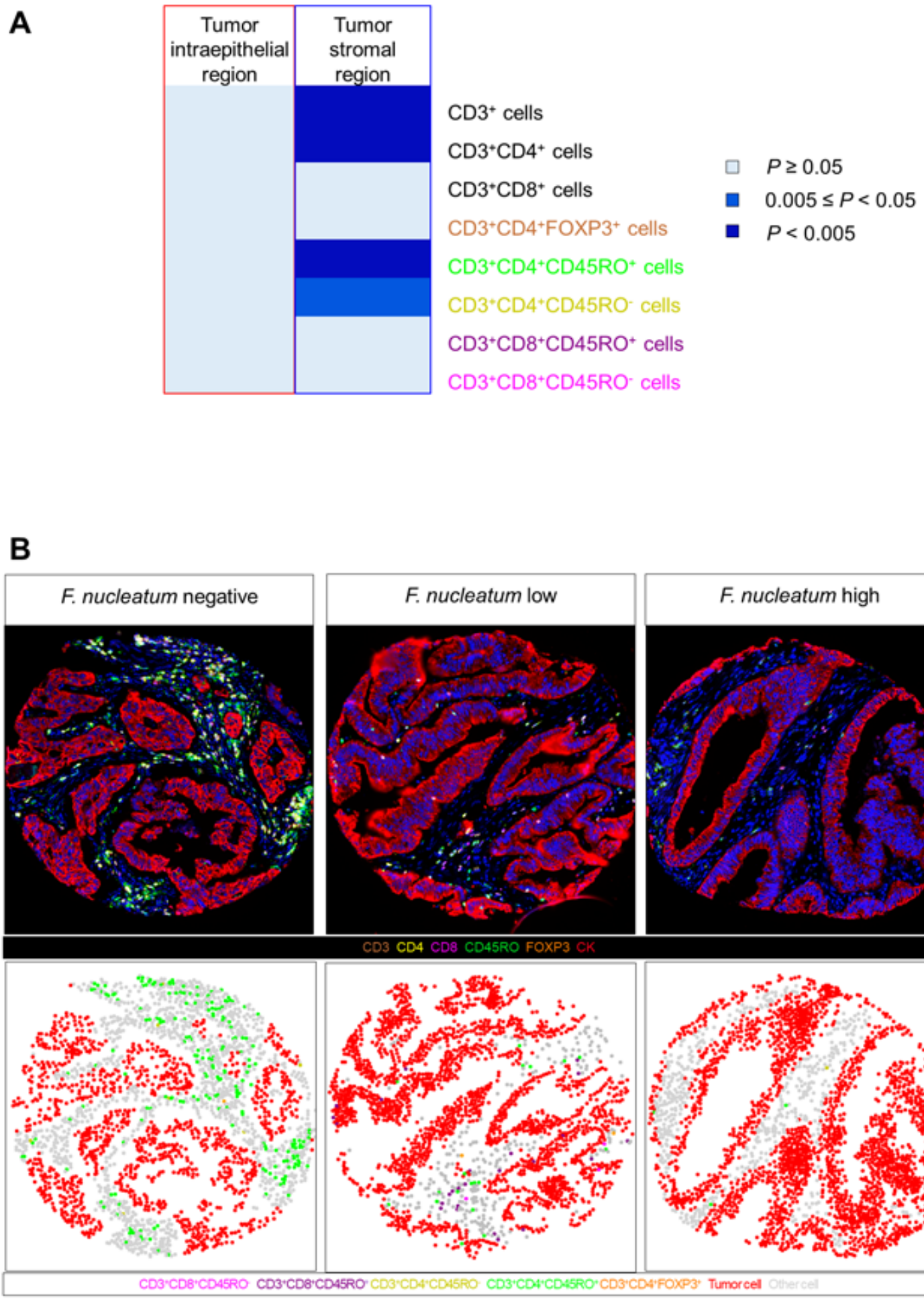

AACR American Association for Cancer Research

Clinical Cancer Research

Association of *Fusobacterium nucleatum* with Specific T Cell Subsets in the Colorectal Carcinoma Microenvironment

Jennifer Borowsky, Koichiro Haruki, Mai Chan Lau, et al.

Clin Cancer Res Published OnlineFirst February 25, 2021.